Atmos. Chem. Phys. Discuss., https://doi.org/10.5194/acp-2017-471
Manuscript under review for journal Atmos. Chem. Phys.
Discussion started: 6 June 2017

Atmospheric Chemistry and Physics Discussions

Three years of measurements of light-absorbing aerosols in the marine air at Henties Bay, Namibia: seasonality, origin, and transport

Paola Formenti[1,$], Stuart John Piketh[2], Andreas Namwoonde[3], Danitza Klopper[2], Mathieu Cazaunau[1], Anaïs Feron[1], Cécile Gaimoz[1], Stephen Broccardo[2], Nicola Walton[2], Karine Desboeufs[1], Guillaume Siour[1], Roelof Burger[2], Mattheus Hanghome[3], Samuel Mafwila[3], Edosa Omoregie[3], Wolfgang Junkermann[4], and Willy Maenhaut[5]

[1] LISA, UMR CNRS 7583, Université Paris Est Créteil et Université Paris Diderot, Institut Pierre Simon Laplace, Créteil, France

[2] School of Geo- and Spatial Science, Unit for Environmental Sciences and Management, North-West University, Potchefstroom, South Africa

[3] Sam Nujoma Marine and Coastal Resources Research Centre (SANUMARC), University of Namibia, Sam Nujoma Campus, Henties Bay, Namibia

[4] Karlsruhe Institute of Technology, Institute of Meteorology and Climate Research, IMK-IFU, Garmisch-Partenkirchen, Germany

[5] Ghent University (UGent), Department of Analytical Chemistry, Gent, Belgium

[$] corresponding author (paola.formenti@lisa.u-pec.fr)

Abstract

Continuous measurements between July 2012 and December 2015 at the Henties Bay Aerosol Observatory (HBAO; 22°S, 14°05'E), Namibia, show that, during the austral wintertime, transport of light-absorbing black carbon aerosols occurs at low-level into the marine boundary layer from the South East Atlantic coast. Daily concentrations reach 986 ng m^{-3} and display a

Atmos. Chem. Phys. Discuss., https://doi.org/10.5194/acp-2017-471
Manuscript under review for journal Atmos. Chem. Phys.
Discussion started: 6 June 2017

Atmospheric Chemistry and Physics Discussions

seasonal maximum from May to August, ahead of the dry season peak of biomass burning in southern Africa (August to October). This outflow is due to either anti-cyclonic circulation or along-the-coast streamlines and contributes to the transport of both biomass and fossil fuel burning aerosols. We estimate that the particle number concentration associated with this transport could contribute up to 2000 cm^{-3} to the cloud droplet number concentration with respect to pristine conditions. Their direct radiative effect is negligible.

1. Introduction

Aerosol particles of natural and anthropogenic origin affect the Earth climate and modulate the greenhouse effect of long-lived gases (Boucher et al., 2013). The extent of the modulation depends on their nature, in particular on their chemical composition and size distribution determining their interactions with radiation and clouds. Current understanding suggests that at the global scale atmospheric aerosols cause an increase of outgoing shortwave radiation, enhancing the atmospheric albedo, thereby counteracting the warming effect of greenhouse gases. However, light-absorbing aerosols, such as black carbon (BC) from fossil fuel and biomass combustion, could reduce the amount of outgoing radiation at the top of atmosphere, finally adding to the greenhouse effect (Haywood and Shine, 1995; Jacobson, 2001; Chung and Seinfeld, 2002; Bond and Bergstrom, 2006; Koch and Del Genio, 2010; Bond et al., 2013). Keil and Haywood (2003) and Koch and Del Genio (2010) have demonstrated that the heating radiative effect of black carbon aerosols might be either enhanced or suppressed when they are above or below clouds, respectively. Additionally, the local heating induced by light-absorption below clouds could modify the cloud properties by enhancing the vertical motion and increasing the cloud cover and liquid water content (Koch and Del Genio, 2010). The entrainment of BC into clouds could cause the cloud to evaporate and rise (Hansen et al., 1997), but could also result in portions of the clouds having smaller mean drop size diameters, higher droplet concentrations and therefore, higher reflectivity (Seinfeld and Pandis, 1997).

In this paper we present long-term observations of black carbon aerosol concentrations at the Henties Bay Aerosol Observatory (HBAO; 22°S, 14°05'E), on the south-east Atlantic coast of Namibia.

The region is pointed out as a hot-spot where global climate models diverge when trying to estimate the top of the atmosphere radiative effect (Myhre et al., 2013). It is characterised by persistent stratocumulus clouds topping a shallow, stable marine boundary layer maintained by the cool sea-surface temperatures of the Benguela Current (Cook et al., 2004; Tyson and Preston-Whyte, 2002). Stratocumulus clouds are highly reflective and modify the net radiative balance at the top of the atmosphere more than any other cloud regimes. Yet, these cloud formations are also amongst the largest source of uncertainty in estimates of the radiative budget of the Earth's atmosphere (Boucher et al., 2013). Nevertheless, the extent to which the aerosols could be entrained and affect the cloud properties in the region is, to date, largely unknown (Kiel and Haywood, 2003).

Henceforth, in this paper we examine the magnitude, the seasonality, and the transport patterns of the black carbon aerosol concentrations measured between July 2012 and December 2015, and we discuss their atmospheric relevance in terms of direct and indirect radiative effects on the stratocumulus cloud deck.

2. Methods

2.1. Measurements of light optical attenuation

Since 2012, surface observations of aerosol particles are conducted at the Henties Bay Aerosol Observatory (HBAO, www.hbao.cnrs.fr), recently accepted as a regional station in the Global Atmosphere Watch (GAW) Programme of the World Meteorological Organization (WMO). The research centre is located on the Sam Nujoma Marine and Coastal Resources Research Centre (SANUMARC) of the University of Namibia in Henties Bay (22°S, 14°05'E), Namibia (**Figure 1**). The campus lies by the coast approximately 100 m from the shore line. To the east

are the Namibian Gravel Plains, to the south is the town of Henties Bay, and to the north is the Omaruru Riverbed (River mouth approximately 100 m from SANUMARC). The population of Henties Bay ranges between 4 600 and 6 000 inhabitants, according to the Namibia 2011 population and housing census (Main Report available at http://cms.my.na/assets/documents/p19dmn58guram30ttun89rdrp1.pdf).

The instruments at HBAO operate from a roof terrace at approximately 30 m above the ground. The terrace hosts the sampling inlets, from which air is drawn into a laboratory room located underneath by straight stainless-steel pipes to avoid particle losses.

The optical attenuation of light (ATN) by aerosol particles smaller than 1 µm in equivalent aerodynamic diameter is measured by a single-wavelength aethalometer (model AE-14U, Magee Sci., Berkeley, CA) operating at 880 nm and sampling at 3.5 (± 0.1) L min^{-1} from a certified PM_1 inlet (BGI Inc., Waltham, MA). A detailed description of the measurement technique is presented in Hansen et al. (1984). Aerosol particles are collected on a quartz fibre tape whilst the light transmittance through the laden filter is measured. Measurements are performed at a 5-min time resolution and stored on a data logger (model CR-1000, Campbell Sci. Ltd.).

The operational algorithm of the aethalometer converts the measured ATN at 880 nm into an estimate of the mass concentration of equivalent black carbon (eBC, in units of mass per volume of sampled air) according to the equation

$$\mathrm{eBC} = \frac{A}{V}\frac{\mathrm{ATN}}{\sigma_{\mathrm{BC}}} \quad (1)$$

where A represents the area of the aerosol deposit on the filter, V the sampled air volume, and σ_{BC} the optical mass absorption cross-section of black carbon (also referred to as the "Specific Attenuation" or mass absorption efficiency), with units of $m^2\ g^{-1}$.

This operational conversion is based on the assumption that black carbon is the strongest light absorbing particulate species in the near infrared. As a matter of fact, Kirchstetter et al. (2004) reported that the mass absorption cross-section of light-absorbing organic carbon in biomass burning samples from southern Africa is nil above 700 nm. At 850 nm, Caponi et al. (2017) reported that the mass absorption cross-section of mineral dust from the Namib Desert is $3\ 10^{-3}$ $m^2\ g^{-1}$ for particles smaller than 2.5 µm in diameter, implying that mineral dust concentrations in the fine size fraction should systematically exceed 1000 µg m^{-3} to cause equivalent absorption.

By default, in the operational aethalometer algorithm the black carbon absorption cross-section σ_{BC} at 880 nm is set to 16.6 $m^2\ g^{-1}$ (Hansen, 2005). This value is based on a calibration factor originally derived in the early 1980's and published by Gundel et al. (1984). However, many authors report on the variability of the mass absorption cross-section related to the chemical state and age of black carbon aerosols (Liousse et al., 1993; Petzold et al., 1997; Martins et al., 1998; Kirchstetter et al., 2003; Hansen, 2005; Bond and Bergstrom, 2006; Knox et al., 2009; Subramian et al., 2010; Bond et al., 2013; Zanatta et al., 2016). Amongst those, Liousse et al. (1993) suggested a value of 20 $m^2\ g^{-1}$ at 550 nm for savannah burning, corresponding to 12.5 $m^2\ g^{-1}$ at 880 nm, when an inverse dependence on wavelength across the visible spectrum is assumed. Kirchstetter et al. (2003) also reported a value of 20 $m^2\ g^{-1}$ at 890 nm for biomass burning in southern Africa. Martins et al. (1998) suggest a mean value of 12.1 (± 4.0) $m^2\ g^{-1}$ at 550 nm for biomass burning in the Brazilian Amazon. More recently, Bond et al. (2013) synthetized the body of published values into a global average of 7.5 (± 1.2) $m^2\ g^{-1}$ at 550 nm. In the absence of a more direct way of constraining the variability that could be due to aging or

source, our best-guess estimate for σ_{BC} in this work is 4.6 (± 0.8) $m^2 g^{-1}$ by extrapolating at 880 nm the mean value of Bond et al. (2013). In the following discussion, the relative uncertainty on σ_{BC} is included in the error estimate for eBC.

Prior to the conversion into eBC (Equation 1), the measured ATN was corrected for multiple scattering (C_{ref} parameter = 2.14 ± 0.21) and shadowing effect (R parameter = 0.93) according to the formulation provided in Weingartner et al. (2003).

2.2. Supporting data

Three-dimensional air mass back trajectories were calculated using the NOAA HYbrid Single-Particle Lagrangian Integrated Trajectory Model (HYSPLIT; Draxler and Rolph, 2015). The model uses the 1°×1° latitude-longitude grid, reanalysis meteorological database. The 6-hourly reanalysis archive data are generated by the NCEP's GDAS (NCEP: National Centers for Environmental Prediction; GDAS: Global Data Assimilation System) wind field reanalysis. Further information can be found at https://rda.ucar.edu/datasets/ds083.2/.

To supplement the back trajectory calculations, hand-drawn synoptic maps of surface meteorological conditions (South African Weather Service, 2016; in the following SAWS, 2016) were used to classify the air motions and climatology linked to aerosol transport towards the site.

3. Results

3.1. Concentrations and seasonality of black carbon aerosols

The daily-averaged eBC mass concentrations measured at HBAO during the study period are shown in **Figure 2**. Values showed a large range of variability from very clean conditions (eBC of the order of 10 ng m^{-3}) to episodic occurrences when mass concentrations exceeded 100 ng m^{-3} and displayed peak values up to 986 ng m^{-3}. We define "excess eBC mass concentrations" the occurrences when the daily eBC concentrations at the site exceeded 100 ng m^{-3}. The mean

value for the whole observing period (July 2012-December 2015) is 92 (± 97) ng m^{-3}. This value and the associated standard deviation are comparable in magnitude to those measured in remote regions of the world impacted by long-range transport of combustion aerosols (**Table 2**). Note that the comparison could be biased by differences in the assumed σ_{BC} values, which are not systematically reported in the quoted papers. Remarkable is the good agreement with the observations of Andreae et al. (1995) on a research cruise over the south east Atlantic along the 19°S meridian off southern Africa, that is, north of our sampling site. Using σ_{BC} = 10 m^2 g^{-1} as specific extinction at 880 nm, these authors showed that black carbon aerosol concentrations in the marine boundary layer increased adjacent to Africa, indicating a strong continental influence (mass concentrations in the range 50-150 ng m^{-3}) in this otherwise pristine environment (mass concentrations lower than 50 ng m^{-3}). On the other hand, the surface concentrations measured at HBAO are lower than those reported for the free troposphere above the stratocumulus cloud deck. During the SAFARI 2000 campaign, mass concentrations of eBC in lofted aged haze from biomass burning were in the range 0.1-6 µg m^{-3} (Kirchstetter et al., 2003; Formenti et al., 2003; Eatough et al; 2003), whereas values up to 5-40 µg m^{-3} were measured in fresh biomass smoke plumes (Kirchstetter et al., 2003).

There is an apparent seasonal variability of the measured eBC at Henties Bay (Figure 2). Concentrations peak in the austral winter from May to September, and are at a minimum from October to April. The observed seasonality is somewhat surprising in that it precedes the seasonal maximum of the biomass burning fire season in southern Africa, peaking in the austral dry season from August to October (Swap et al., 2002). Nonetheless, various facts indicate that a local contamination cannot be at the origin of the observed excess eBC mass concentrations. First of all, Henties Bay, 3 km to the south-east of the sampling site of the University campus, is a small town in an arid environment with no vegetation, no industrial activity and very little traffic. Energy usage is by a mix of electricity and gas, whereas little use is made of solid fuel

combustion due to low availability. Secondly, the data have been screened on the basis of the time variability of concentrations increasing and then decreasing to the background values in one-two hour time intervals. Episodes with these characteristics were observed on a few occasions, for example for New Year's Eve, and are associated with open fires for barbequing meat. On the contrary, the peaks of eBC in the May-to-August period are long-lasting, extending on average between 6 and 11 hours on peak days, and occurring during both day- and night-time. The possible factors explaining the magnitude and the unexpected seasonal variability in the observed eBC mass concentrations are examined in the following sections.

3.2. Transport patterns and links to synoptic scale circulation

3.2.1. Characteristics of the regional synoptic circulation

We examine here the changes in the synoptic circulation induced by diurnal and seasonal cycles, which could affect the transport of aerosols to Henties Bay. **Figure 1.S** shows examples of the typical (most prevalent) synoptic conditions to be expected for summer and winter (SAWS, 2016). The iso-contours are highlighted to illustrate the relative positions of the pressure bands at the surface, during the different seasons. The tropical low pressure system, which is centred on the north/northeast of Namibia throughout the year, however with varying intensity, is commonly known as an easterly low and is sometimes referred to as a tropical or Angolan/Namibian low (Cook et al., 2004). Typically, in the summer, when the easterly low joins the low pressures of the westerly wave, a tropical temperate trough will form. Due to instability along the central line of this trough, cloud bands will form. The air masses behind the trough, along the West Coast, will undergo surface divergence which does not lead to the development of rainfall. During the winter time, a band of suppressed convection forms between the weak low pressure and the SE Atlantic High, and the atmosphere over the West Coast is subject to subsidence and divergence at the surface over the ocean, which inhibits convection and rainfall (Cook et al., 2004).

The weather patterns observed in Henties Bay arise from its proximity to the coast and location between the tropics and middle latitudes. The prevailing surface winds are associated with the trade winds which occur at low levels in the troposphere and are responsible for the mean circulation in this region (Taljaard, 1994; Preston-Whyte and Tyson, 1988; Tyson and Preston-Whyte, 2002). The meridional mean for the West Coast is southerly flow. To the east of the subtropical South Atlantic anticyclone, southerly to easterly trade winds blow with high consistency and the system strengthens during the wintertime as surface pressures increase. When the amplitude of the Westerly Wave is at its highest in the peak of winter (due to the northward retreat of the Inter Tropical Convergence Zone), the airflow effectively changes from easterly (summer) to northerly (winter) along the West Coast (Taljaard, 1994).

The local conditions remain conducive to a stable boundary layer where local mixing is driven by diurnal land- and sea breezes. During the summer enhanced upwelling may result in colder water temperatures with respect to the warmer desert surface and instead of inducing a land breeze at night, it could sustain the sea breeze and therefore onshore transport of aerosols (Oke, 1987). Finally, as in other coastal regions, the atmospheric boundary layer depth at Henties Bay varies less than over the interior of southern Africa (Preston-Whyte et al., 1988). The height of the first non-surface inversion base over the west coast is typically 1000 m above sea level (asl) during winter and 500 m asl in summer (Tyson and Preston-Whyte, 2002). It is worth noting that the seasonal difference of the boundary layer height, also associated with the changes in synoptic regimes, is opposite to the seasonal cycle of the BC concentrations.

3.2.2. Links between synoptic circulation and air mass trajectories

In order to establish the origin of the elevated eBC occurrences in Henties Bay, and their link to the dominant transport patterns and synoptic scale features (< 1000 m horizontal scale), three-day back trajectories ending at HBAO have been calculated for days when the daily eBC concentrations at the site exceeded 100 ng m^{-3}.

A case study approach was taken to group trajectories into 12 envelopes (**Figure 2.S** in the supplementary material) which best describe typical air parcel patterns travelling towards HBAO. According to the main source regions of the air masses, the envelopes were further divided into 3 groups, namely Atlantic flow (Figure 3a), south-easterly continental flow (Figure 3b) and easterly continental flow (Figure 3c).

Air masses transported within the Atlantic flow pathways were the most frequent. They originated over the Atlantic Ocean, between 30°S and 55°S. These air masses are generally driven north-east or east by the westerly wave, then deflected by the continental ridge and driven along the coast towards the easterly low north of Henties Bay. Generally, trajectories which travelled further are linked to strong pressure gradients of the westerly wave. In some cases ridging highs extend across the south of South Africa, blocking air masses in the south from reaching Henties Bay. The easterly low located over and north of Henties Bay draws air masses in from the northwest, off the coast of northern Namibia and Angola.

Air masses of the easterly continental flow pathway were observed to travel mainly along trajectories between 15°S and 22°S. The synoptic patterns which dominate this transport pathway are a combination of approaching cold fronts, the presence of the easterly low over the north of Namibia, ridging highs over the south and east of South Africa and relatively higher pressures in the Indian than in the Atlantic Ocean.

The synoptic patterns of the south-easterly continental flow pathway are characterised by lower pressures in the Southeast Atlantic, and relatively lower pressures inland than to the east of the subcontinent. The air masses are driven westwards and deflected north by approaching cold fronts. In some cases ridging highs extend across the south of South Africa and can lead to regional recirculation. These air masses are of mainly continental origin and are concentrated between 20°S and 30°S.

Figure 4 shows the frequency of trajectories with excess eBC mass concentrations arriving at HBAO from the 3 major flow pathways. Over the period of 2012 to 2015, 60% of the air masses contributing to excess eBC travelled over the Atlantic Ocean. Only 40% of these air masses travelled entirely over land, divided into 15% in the south-easterly flow and 25% in the easterly continental flow.

3.2.3. Contribution of air transport patterns to excess eBC mass concentrations

In order to estimate the contribution of continental and Atlantic air masses to excess eBC mass concentrations, daily eBC mass concentrations higher than 100 ng m^{-3} were sorted and classified according to the air mass origin. The statistics summary is reported in **Table 2**. **Figure 5** shows the results of this classification as box and whisker plots. At a first impression, the range of variability of the BC concentrations is very similar. A closer look, however, shows that the distribution of values is different. **Figures 3.S** and **4.S** in the supplementary material show that air masses in the Atlantic flow have, on average, a lower mass concentration than continental air masses, and excess concentrations are mostly due to outliers: 90% of the eBC mass concentration values of the Atlantic group are smaller than 250 ng m^{-3}. Only 10% of the values are above 250 ng m^{-3}, with only two observations resulting in extreme values higher than 550 ng m^{-3}. On the contrary, the average mass concentration of the continental air masses is systematically higher: 90% of the values reach up to 450 ng m^{-3} in the easterly continental pathway (trajectories G5-G12) and in the south-easterly continental pathway (trajectory groups G8-G10).

These observations are confirmed by a student-t statistical test on the results, showing that the mean mass concentration of excess eBC for the Atlantic group (G1-G4) is significantly lower (at 0.01 confidence level) than those of the continental flow pathways, whereas the G8-G10 and G5-G12 grouping significantly differ only at the 0.05 confidence level.

Atmos. Chem. Phys. Discuss., https://doi.org/10.5194/acp-2017-471
Manuscript under review for journal Atmos. Chem. Phys.
Discussion started: 6 June 2017

4. Atmospheric relevance

Our observations indicate that, in the marine boundary layer of coastal Namibia, the synoptic circulation is responsible for the long-range transport of polluted air masses whose mass concentrations of (equivalent) black carbon aerosols exceed the background levels by up to a factor of 10. The relevance of their potential impacts on the local radiative budget, by direct extinction or by modifying the properties of clouds, can be evaluated by estimating the order of magnitude of their aerosol optical depth (AOD) and cloud droplet number concentration (CDNC).

An estimate of AOD in the mid-visible (e.g., 550 nm) can be evaluated as

$$AOD_{550\ nm} = \frac{eBC}{f_m}\ \sigma_{e,550\ nm}\ \Delta z \qquad (2)$$

where

- eBC is the mean mass concentration of excess eBC estimated from our observations (205 ± 130 ng m^{-3}).

- f_m is the mass fraction of black carbon to the total aerosol mass, set to the upper limit value of 10% (Bond et al., 2013)

- $\sigma_{e,550\ nm}$ is the mass extinction cross-section at 550 nm (4.6 $m^2\ g^{-1}$) of biomass burning aerosols containing black carbon from Haywood et al. (2013)

- Δz is the depth of the aerosol layer supposed as well mixed up to the upper edge of the boundary layer, set to 700 m above sea level according to Keil and Haywood (2003).

The resulting mean AOD would not exceed 0.01, negligible with respect to the mean AOD of 0.2-0.4 reported by the collocated AERONET sunphotometer during the peak of the fire season

(not shown). These occurrences should not contribute to any significant direct and semi-direct radiative effects. However, that the long-range transported black carbon could significantly contribute to an enhancement of the cloud droplet number concentration (CDNC) by up to 2000 cm^{-3}, consistent to measurements in other remote regions of the world, such as Eastern Australia (Junkermann and Hacker, 2015). This evaluation is based on the empirical linear relationship between the peak cloud droplet number concentration (CDNC) in the stratocumulus decks and the corresponding concentration of accumulation mode particles just below cloud base established by Hegg et al. (2012) through the analysis of published data, including Namibia. This relationship averages out the broad range of aerosol hygroscopicity in the particle accumulation mode, therefore the dependence on supersaturation conditions. For our purpose, the cloud droplet number concentration (CDNC) can be calculated as

$$CDNC = a\ x\ AMNC = a\ x\ (\mathrm{eBC}\ x\ b) \quad (3)$$

where

- The a parameter (equal to 0.80 ± 0.03) is obtained by restricting the proportionality factor obtained by Hegg et al. (2012) to observations offshore Namibia. Hegg et al. (2012) calculated the proportionality factor from the linear regression (R^2 = 0.98) of simultaneous measurements of cloud droplet number concentration (CDNC) in clouds to the accumulation mode number concentration (AMNC) below clouds
- The b value is the proportionality factor of 14 cm^{-3} $(ng\ C\ m^{-3})^{-1}$ obtained by Andreae et al. (1995) in our study area and relating the equivalent black carbon mass concentrations (eBC) and AMNC

For the mean mass concentration of excess eBC estimated in this study (205 ± 130 ng m^{-3}), the CNDC values estimated from Equation 3 reach 2000 cm^{-3}, therefore exceeding by a factor of 40 the number concentration of ~50 cm^{-3} reported for pristine clouds (Keil and Haywood, 2003).

5. Conclusions

We have presented the first long-term time series of surface observations of black carbon aerosols along the south-east Atlantic coast offshore southern Africa. These observations were conducted at the Henties Bay Aerosol Observatory (HBAO), Namibia, between July 2012 and December 2015. The main conclusion of this study are

- Light-absorbing aerosols that can be identified as black carbon containing aerosols are transported at low-level in the marine boundary layer on the south-east Atlantic coast with mass concentrations averaging 92 (± 97) ng m^{-3} over the July 2012-December 2015 study period. Occurrences of peak mass concentrations exceed the background mass concentrations (estimated in the range 20-50 ng m^{-3}) by up to a factor of 20, reaching 800-900 ng m^{-3}, and averaging at 205 (± 130) ng m^{-3}. This range of values is in agreement with previous measurements in remote areas of the world impacted by long-range transport of pollutants, and in particular with the intensive observations of Andreae et al. (1995) in the same area during a research cruise along the 19°S meridian. Indeed, as the specific attenuation used in calculating the concentrations of black carbon from optical attenuation measurements are different, comparisons have to be considered as indicative. The mean specific attenuation used in this paper is lower by a factor of two than that used by Andreae et al. (1995), who, however, sampled about 300 km north of HBAO where concentrations could be naturally higher as in the maximum of the outflow of continental polluted air masses (Swap et al., 1992). On the other hand, the mass concentrations in the marine boundary layer presented in this paper are

significantly lower than those reported for the same geographical region for biomass burning layers transported aloft the stratocumulus cloud deck (Haywood et al., 2003; Kirchstetter et al., 2003; Formenti et al., 2003; Eatough et al; 2003).

- The transport of the eBC-rich air masses described in this paper has a marked seasonal cycle in the austral wintertime between May and August. It occurs ahead of the peak of the dry season for southern Africa (August to October), when the major outflow of biomass burning aerosols takes place (Swap et al., 2002; Haywood et al., 2003). Based on the analysis of streamline back-trajectories and active fire count maps, we believe that the enhanced eBC mass concentrations measured at the site are due to the low-level transport of continental combustion aerosols, either from biomass burning or from fossil fuel burning. The existence of two major transport patterns (anticyclonic recirculation and along-the-coast streamlines) suggests that the possible sources of black carbon aerosols include biomass burning in southern and central Africa, industrial sources in the South African Highveld (Piketh et al., 2002), but also emissions from shipping routes along the west coast (Tournadre, 2014; Fraser et al., 2016).
- The aerosol optical depth associated to the low-level eBC aerosols is within 0.01 at 550 nm, with large uncertainties due to the estimate of optical properties. Their direct radiative effect should be insignificant. However, these aerosols could be entrained into the stratocumulus clouds, where their indirect effect might matter (Keil and Haywood, 2003). The entrainment of boundary layer aerosols into the stratocumulus clouds is favoured by the turbulent mixing of air below 2 km induced by eddies generated by land and sea breezes driven by thermal winds (Preston-Whyte and Tyson, 1988), whereas, on the contrary, the large temperature inversion at the cloud top (up to 16 K) mostly inhibits the entrainment of lofted layers, at least close to the coast (Kiel and Haywood, 2003; Haywood et al., 2003). Using an empirical relationship relating the number of

droplets in clouds to the number of accumulation particles below clouds (Hegg et al., 2012), we also estimate that the cloud droplet number concentration provided by the eBC-aerosol layers entrained into the stratocumulus cloud deck could increase by up to a factor of 40 compared to that of cloud droplets in pristine conditions. Clearly we do not want to presume further on the relevance of the possible effects of the eBC-enriched aerosols on the stratocumulus cloud deck, which will require a much more extensive set of observations and dedicated modelling. It should be noted also that the pertinence to polluted air masses of the empirical relationship by Hegg et al. (2012), which is well in agreement with previous findings by Andreae et al. (1995) of clean air where DMS oxidation was the major particle source, remains to be proven.

- These pioneering measurements are informative of concentrations of polluted air masses as well as of an additional transport route of aerosols in the boundary layer. However, they have limitations which prevent more firm results and conclusions. Near-future observations, ground-based and airborne, foreseen in the area in the framework of large scale international projects, should provide detailed data sets of size-resolved measurements of the aerosol number and mass concentration and composition. This will help remove some of the more speculative aspects of our current results, and will provide guidance in the further investigation of the effect of the low-level aerosol forcing on the cloud properties on the long-time scale.

Acknowledgments

This work receives funding by the French Centre National de la Recherche Scientifique (CNRS) and the South African National Research Foundation (NRF) through the "Groupement de Recherche Internationale Atmospheric Research in southern Africa and the Indian Ocean" (GDRI-ARSAIO) and the Projet International de Coopération Scientifique (PICS) "Long-term observations of aerosol properties in Southern Africa" (contract n. 260888) as well as by the

389 Partenariats Hubert Curien (PHC) PROTEA of the French Ministery of Foreigns Affairs and
390 International Development (contract numbers 33913SF and 38255ZE).

391 We acknowledge the use of the HYSPLIT model from the NOAA Air Resources Laboratory
392 (ARL). Original data can be obtained by email request to the first author of this paper.

393 **References**

394 Andreae, M. O., W. Elbert, and S. J. de Mora, Biogenic sulfur emissions and aerosols
395 over the tropical South Atlantic: 3. Atmospheric dimethylsulfide, aerosols and cloud
396 condensation nuclei, J. Geophys. Res. Atmospheres, 100(D6), 11335-11356, 1995.

397 Bodhaine, B. A., Aerosol absorption measurements at Barrow, Mauna Loa, and South
398 Pole, J. Geophys. Res., 100, 8967–8975, 1995.

399 Bond, T. and R. W. Bergstrom, Light Absorption by Carbonaceous Particles: An
400 Investigative Review, Aerosol Sci. Technol., 39:1–41, doi: 10.1080/02786820500421521,
401 2006.
402 Bond, T. C., et al., Bounding the role of black carbon in the climate system: A
403 scientific assessment, J. Geophys. Res. Atmos., 118, 5380–5552, doi:10.1002/jgrd.50171,
404 2013.

405 Boucher, O., D. Randall, P. Artaxo, C. Bretherton, G. Feingold, P. Forster, V.-M.
406 Kerminen, Y. Kondo, H. Liao, U. Lohmann, P. Rasch, S.K. Satheesh, S. Sherwood, B. Stevens
407 and X.Y. Zhang, 2013: Clouds and Aerosols. In: Climate Change 2013: The Physical Science
408 Basis. Contribution of Working Group I to the Fifth Assessment Report of the
409 Intergovernmental Panel on Climate Change [Stocker, T.F., D. Qin, G.-K. Plattner, M. Tignor,
410 S.K. Allen, J. Boschung, A. Nauels, Y. Xia, V. Bex and P.M. Midgley (eds.)]. Cambridge
411 University Press, Cambridge, United Kingdom and New York, NY, USA, pp. 571–658,
412 doi:10.1017/CBO9781107415324.016.

413 Caponi, L., Formenti, P., Massabó, D., Di Biagio, C., Cazaunau, M., Pangui, E.,
414 Chevaillier, S., Landrot, G., Andreae, M. O., Kandler, K., Piketh, S., Saeed, T., Seibert, D.,
415 Williams, E., Balkanski, Y., Prati, P., and Doussin, J.-F.: Spectral- and size-resolved mass
416 absorption efficiency of mineral dust aerosols in the shortwave: a simulation chamber study,
417 Atmos. Chem. Phys. Discuss., doi:10.5194/acp-2017-5, in review, 2017.

418 Chung, S. H. and J. H. Seinfeld, Global distribution and climate forcing of carbonaceous
419 aerosols, Journal of Geophysical Research: Atmospheres, 107(D19), AAC 14-11-AAC 14-33,
420 2002.

421 Cook, C., Reason, C.J.C. and B.C. Hewitson, Wet and dry spells within particularly wet
422 and dry summers in the South African summer rainfall region. Climate Research, 26(1), 17–31,
423 2004.

424 Derwent, R. G., D. B. Ryall, S. G. Jennings, T. G. Spain, and P. G. Simmonds, Black
425 carbon aerosol and carbon monoxide in European regionally polluted air masses at Mace Head,
426 Ireland during 1995-1998, Atmos Environ., 35, 6371-6378, 2001.

427 Draxler, R. R. and G. D. Rolph, HYSPLIT (HYbrid Single-Particle Lagrangian
428 Integrated Trajectory) Model access via NOAA ARL READY Website

(http://ready.arl.noaa.gov/HYSPLIT.php). NOAA Air Resources Laboratory, Silver Spring, MD, 2015.

Eatough, D. J., N. L. Eatough, Y. Pang, S. Sizemore, T. W. Kirchstetter, T. Novakov, and P. V. Hobbs, Semivolatile particulate organic material in southern Africa during SAFARI 2000, J. Geophys. Res., 108, 8479, doi:10.1029/2002JD002296, D13, 2003.

Formenti, P., W. Elbert, W. Maenhaut, J. Haywood, S. Osborne, and M. O. Andreae, Inorganic and carbonaceous aerosols during the Southern African Regional Science Initiative (SAFARI 2000) experiment: Chemical characteristics, physical properties, and emission data for smoke from African biomass burning, J. Geophys. Res., 108 (D13), 8488, doi:10.1029/2002JD002408, 2003.

Fraser, D. R., T. Notteboom, and C. Ducruet, Peripherality in the global container shipping network: the case of the Southern African container port system, GeoJournal, 81, 139. doi:10.1007/s10708-014-9610-6, 2016.

Gundel, L. A., R. L. Dod, H. Rosen, and T. Novakov, The relationship between optical attenuation and black carbon concentration for ambient and source particles, The Science of the Total Environment, 36, 197–202. doi: 10.1016/0048-9697(84)90266-3, 1984.

Hansen, A. D. A., The aethalometer, technical guide, 2005; available online at http://www.mageesci.com/images/stories/docs/Aethalometer_book_2005.07.03.pdf)

Hansen, A. D. A., H. Rosen and T. Novakov, The aethalometer - an instrument for the real-time measurement of optical absorption by aerosol particles, Sci. Total Environ., 36, 191, 1984.

Hansen, J. E., Sato, M. and Ruedy, R., Radiative forcing and climate response, J. Geophys. Res., 102, 6831–6864, 1997.

Haywood, J., and K. Shine, The effect of anthropogenic sulfate and soot aerosol on the clear sky planetary radiation budget, Geophys. Res. Lett., 22(5), 603-606, 1995.

Haywood, J. M., S. R. Osborne, P. N. Francis, A. Keil, P. Formenti, M. O. Andreae, and P. H. Kaye, The mean physical and optical properties of regional haze dominated by biomass burning aerosol measured from the C-130 aircraft during SAFARI 2000, J. Geophys. Res., 108 (D13), 8473, doi:10.1029/2002JD002226, 2003.

Hegg, D. A., D. S. Covert, H. H. Jonsson and R. K. Woods, A simple relationship between cloud drop number concentration and precursor aerosol concentration for the regions of Earth's large marine stratocumulus decks, Atmos. Chem. Phys., 12, 1229-1238, doi:10.5194/acp-12-1229-2012, 2012.

Jacobson, M., Strong radiative heating due to the mixing state of black carbon in atmospheric aerosols, Nature, 409(6821), 695-697, 2001.

Johnson, B. T., K. P. Shine, and P. M. Forster, The semi-direct aerosol effect: Impact of absorbing aerosols on marine stratocumulus, Q. J. Roy. Meteorol. Soc., 130, 1407–1422, 2004.

Jones, A., J. Haywood, and O. Boucher, Climate impacts of geo-engineering marine stratocumulus clouds, J. Geophys. Res., 114, D10106, doi:10.1029/2008JD011450, 2009.

Jones, A., and J. M. Haywood, Sea-spray geoengineering in the HadGEM2-ES earth-system model: radiative impact and climate response, Atmos. Chem. Phys., 12, 10887-10898, doi:10.5194/acp-12-10887-2012, 2012.

Junkermann, W., and J. M. Hacker, Ultrafine particles over Eastern Australia: an airborne survey, Tellus B, 67, 25308, http://dx.doi.org/10.3402/tellusb.v67.25308Vol 67, 2015.

473 Keil, A., and J. M. Haywood, Solar radiative forcing by biomass burning aerosol
474 particles during SAFARI 2000: A case study based on measured aerosol and cloud properties,
475 J. Geophys. Res., 108, 8467, doi:10.1029/2002JD002315, D13, 2003.

476 Kirchstetter, T. W., T. Novakov, P. V. Hobbs, and B. Magi, Airborne measurements of
477 carbonaceous aerosols in southern Africa during the dry biomass burning season, J. Geophys.
478 Res., 108, 8476, doi:10.1029/2002JD002171, D13, 2003.

479 Kirchstetter, T. W., T. Novakov, and P. V. Hobbs, Evidence that the spectral dependence
480 of light absorption by aerosols is affected by organic carbon, J. Geophys. Res., 109, D21208,
481 doi:10.1029/2004JD004999, 2004.

482 Knox, A., G. J. Evans, J. R. Brook, X. Yao, C. H. Jeong, K. J. Godri, K. Sabaliauskas,
483 and J. G. Slowik, Mass Absorption Cross-Section of Ambient Black Carbon Aerosol in Relation
484 to Chemical Age, Aerosol Science and Technology, 43(6), 522-532, 2009.

485 Koch, D. and A. D. Del Genio, Black carbon semi-direct effects on cloud cover: review
486 and synthesis, Atmos. Chem. Phys., 10, 7685-7696, doi:10.5194/acp-10-7685-2010, 2010.

487 Liousse, C., H. Cachier, and S. G. Jennings, Optical and thermal measurements of black
488 carbon aerosol content in different environments: Variations of the specific attenuation cross-
489 section, sigma (σ). Atmos. Environ., 27A(8), 1203-1211, 1993.

490 Marinoni, A., P. Cristofanelli, P. Laj, R. Duchi, F. Calzolari, S. Decesari, K. Sellegri, E.
491 Vuillermoz, G. P. Verza, P. Villani, and P. Bonasoni, Aerosol mass and black carbon
492 concentrations, a two year record at NCO-P (5079 m, Southern Himalayas), Atmos. Chem.
493 Phys., 10, 8551-8562, doi:10.5194/acp-10-8551-2010, 2010.

494 Martins, J. V., P. Artaxo, C. Liousse, J. S. Reid, P. V. Hobbs, Y. J. Kaufman, Effects
495 of black carbon content, particle size and mixing on light absorption by aerosol particles from
496 biomass burning in Brazil, J. Geophys. Res., 103, D24, 32041-32050, 1998.

497 Myhre, G., Samset, B. H., Schulz, M., Balkanski, Y., Bauer, S., Berntsen, T. K., Bian,
498 H., Bellouin, N., Chin, M., Diehl, T., Easter, R. C., Feichter, J., Ghan, S. J., Hauglustaine, D.,
499 Iversen, T., Kinne, S., Kirkevåg, A., Lamarque, J. F., Lin, G., Liu, X., Lund, M. T., Luo, G.,
500 Ma, X., van Noije, T., Penner, J. E., Rasch, P. J., Ruiz, A., Seland, Ø., Skeie, R. B., Stier, P.,
501 Takemura, T., Tsigaridis, K., Wang, P., Wang, Z., Xu, L., Yu, H., Yu, F., Yoon, J. H., Zhang,
502 K., Zhang, H., and Zhou, C.: Radiative forcing of the direct aerosol effect from AeroCom Phase
503 II simulations, Atmos. Chem. Phys., 13, 1853-1877, 10.5194/acp-13-1853-2013, 2013.

504 Oke, T.R. Boundary Layer Climates. 2nd ed. Routledge: Taylor and Francis, 1987.

505 Petzold, A., C. Kopp, and R. Niessner, The dependence of the specific attenuation cross-
506 section on black carbon mass fraction and particle size, Atmospheric Environment, 31(5), 661-
507 672, 1997.

508 Piketh, S. J., R. J. Swap, W. Maenhaut, H. J. Annegarn, and P. Formenti, Chemical
509 evidence of long-range atmospheric transport over southern Africa, J. Geophys. Res.,
510 107(D24), 4817, doi:10.1029/2002JD002056, 2002.

511 Preston-Whyte, R.A. and P. D. Tyson, The Atmosphere and Weather of Southern
512 Africa. Cape Town: Oxford University Press, 1988.

513 Seinfeld, J. H. and S. N. Pandis, Eds., Atmospheric chemistry and physics: From air
514 pollution to climate change. New York, John Wiley and Sons, Inc., 1997.

515 South African Weather Service (SAWS), 2016. Publications, Retrieved from
516 http://www.weathersa.co.za/climate/publications.

Subramanian, R., Kok, G. L., Baumgardner, D., Clarke, A., Shinozuka, Y., Campos, T. L., Heizer, C. G., Stephens, B. B., de Foy, B., Voss, P. B., and Zaveri, R. A.: Black carbon over Mexico: the effect of atmospheric transport on mixing state, mass absorption cross-section, and BC/CO ratios, Atmos. Chem. Phys., 10, 219-237, doi:10.5194/acp-10-219-2010, 2010.

Swap, R. J., H. J. Annegarn, J. T. Suttles, J. Haywood, M. C. Helmlinger, C. Hely, P. V. Hobbs, B. N. Holben, J. Ji, M. D. King, T. Landmann, W. Maenhaut, L. Otter, B. Pak, S. J. Piketh, S. Platnick, J. Privette, D. Roy, A. M. Thompson, D. Ward, D. and R. Yokelson, The Southern African Regional Science Initiative (SAFARI 2000) : overview of the dry season field campaign, *South African J. Science*, 98, 125-130, 2002.

Taljaard, J. J., Atmospheric circulation systems, synoptic climatology and weather phenomena of South Africa. Part 1: controls of the weather and climate of South Africa, Technical Paper No. 27, Weather Bureau, Pretoria [available from South African Weather Bureau, Private Bag X097, Pretoria 0001], 1994.

Tournadre, J., Anthropogenic pressure on the open ocean: The growth of ship traffic revealed by altimeter data analysis, *Geophys. Res. Lett.*, 41, 7924-7932, 2014.

Tyson, P. D., and R. A. Preston-Whyte, The Weather and Climate of Southern Africa. Oxford University Press Southern Africa, Cape Town, 2002.

von Schneidemesser, E., J. J. Schauer, G. W. Hagler, and M. H. Bergin, Concentrations and Sources of Carbonaceous Aerosol in the Atmosphere of Summit, Greenland, Atmos. Environ., 43, 4155-4162, 2009.

Weingartner, E., H. Saathoff, M. Schnaiter, N. Streit, B. Bitnar, and U. Baltensperger, Absorption of light by soot particles: determination of the absorption coefficient by means of aethalometers, Journal of Aerosol Science, 34(10), 1445-1463, 2003.

Zanatta, M., Gysel, M., Bukowiecki, N., Müller, T., Weingartner, E., Areskoug, H., Fiebig, M., Yttri, K. E., Mihalopoulos, N., Kouvarakis, G., Beddows, D., Harrison, R. M., Cavalli, F., Putaud, J. P., Spindler, G., Wiedensohler, A., Alastuey, A., Pandolfi, M., Sellegri, K., Swietlicki, E., Jaffrezo, J. L., Baltensperger, U., and Laj, P.: A European aerosol phenomenology-5: Climatology of black carbon optical properties at 9 regional background sites across Europe, Atmospheric Environment, 145, 346-364, https://doi.org/10.1016/j.atmosenv.2016.09.035, 2016.

548 **Table captions**

549 **Table 1.** Values of mass concentrations of equivalent black carbon eBC from measurements
550 published in the literature for remote regions worldwide. When available, the specific
551 attenuation used to convert the measured attenuation to eBC is also reported.

552 **Table 2.** Summary statistics of daily averaged equivalent black carbon aerosol concentration
553 (eBC) sorted by air mass origin. The mean, standard deviation, range between minimum and
554 maximum concentrations and range between the 25% and the 75% percentiles are expressed in
555 ng m^{-3}.

556 **Figure captions**

557 **Figure 1.** Geographical location of the Henties Bay Aerosol Observatory (HBAO).

558 **Figure 2.** Time series of daily average equivalent black carbon mass concentration (eBC)
559 calculated from the processed 5-min data. Error bars represent the standard deviations of daily
560 concentrations, by far exceeding the analytical error on the data reduction.

561 **Figure 3.** Classification of air masses corresponding to occurrences of eBC exceeding 100 g
562 m^{-3} (excess eBC) according to the main source regions: top left: Atlantic flow (trajectory groups
563 G1-G4); top right: south-easterly continental flow (trajectory groups G8-G10); bottom left:
564 easterly continental flow (trajectory groups G5-G12).

565 **Figure 4.** Yearly frequency distribution of trajectory pathways in the Atlantic group (blue),
566 south-easterly continental group (orange) and easterly continental flow (grey) for the study
567 period (July 2012-December 2015).

568 **Figure 5.** Box and whisker plot of the frequency distribution of values of the excess mass
569 concentration of equivalent black carbon (excess eBC) measured for each flow path, Atlantic
570 (blue), south-easterly continental (orange), and easterly continental (grey), from left to right.
571 Boxes depict the 25%, the 50% (median) and the 75% percentiles. The open square represents
572 the mean of the distribution, whereas the whiskers represent the minimum and maximum values
573 of the distributions.
574

Table 1. Values of mass concentrations of equivalent black carbon eBC from measurements published in the literature for remote regions worldwide. When available, the specific attenuation σ_{BC} used to convert the measured attenuation to eBC is also reported.

Location	eBC (ng m^{-3})	σ_{BC}, 880 nm (m^2 g^{-1})	Reference
Tropical South Atlantic off southern Africa, 19°S	50-150	10	Andreae et al. (1995)
Nepal Climate Observatory Pyramid, Himalaya	160 ± 296	6.5[$]	Marinoni et al. (2010)
Summit, Greenland	<340	-----	von Schneidemesser et al. (2009)
Mace-Head, Ireland	47-74	11 ± 3	Derwent et al. (2001)
South Pole, Antarctica	0.01-50	19	Bodhaine (1995)

[$] At 635 nm – measurements were conducted with a Multi-Angle absorption Photometer (MAAP 5012, Thermo Electron Corporation)

Atmos. Chem. Phys. Discuss., https://doi.org/10.5194/acp-2017-471
Manuscript under review for journal Atmos. Chem. Phys.
Discussion started: 6 June 2017

Atmospheric Chemistry and Physics Discussions

582 **Table 2.** Summary statistics of excess daily black carbon equivalent aerosol concentration
583 (eBC) sorted by air mass origin. The mean and standard deviation, the range between minimum
584 and maximum concentrations and the range between the 25% and the 75% percentiles are
585 expressed in ng m^{-3}.

586

	Mean ± standard deviation	Range (min-max)	Range (25%-75% percentile)	Number of data points
G1-G4	189 ± 94	101-750	131-214	112
G5-G12	272 ± 146	106-889	161-349	77
G8-G10	324 ± 141	112-639	210-418	25

587
588

Atmos. Chem. Phys. Discuss., https://doi.org/10.5194/acp-2017-471
Manuscript under review for journal Atmos. Chem. Phys.
Discussion started: 6 June 2017

Atmospheric Chemistry and Physics Discussions

589 **Figure 1:** Geographical location of the Henties Bay Aerosol Observatory (HBAO).

590

591

Atmos. Chem. Phys. Discuss., https://doi.org/10.5194/acp-2017-471
Manuscript under review for journal Atmos. Chem. Phys.
Discussion started: 6 June 2017

Atmospheric Chemistry and Physics Discussions

592 **Figure 2:** Time series of daily average black carbon mass concentration (eBC) calculated from
593 the processed 5-min data. Error bars represent the standard deviations of daily concentrations,
594 by far exceeding the analytical error on the data reduction.

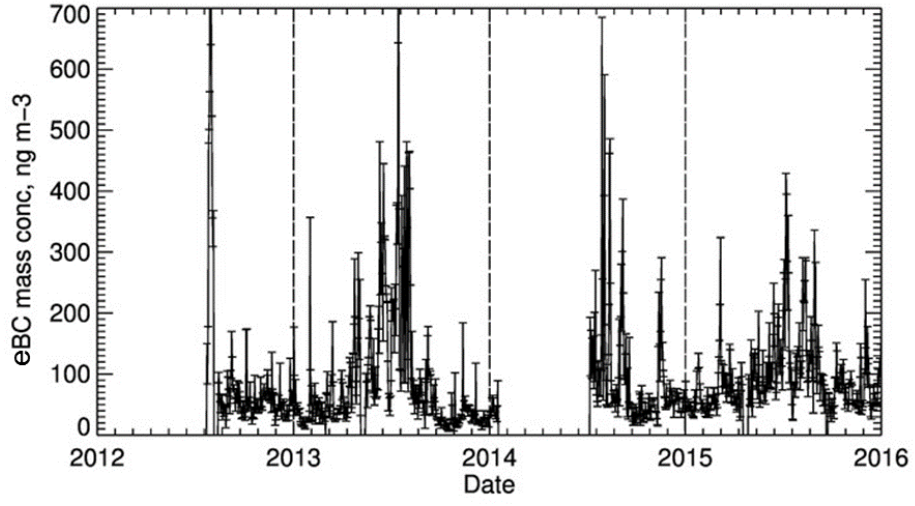

595
596

Atmos. Chem. Phys. Discuss., https://doi.org/10.5194/acp-2017-471
Manuscript under review for journal Atmos. Chem. Phys.
Discussion started: 6 June 2017

Atmospheric Chemistry and Physics Discussions

597 **Figure 3.** Classification of air masses corresponding to occurrences of eBC exceeding 100 g m^{-3}
598 (excess eBC) according to the main source regions: top left: Atlantic flow (trajectory groups
599 G1-G4); top right: south-easterly continental flow (trajectory groups G8-G10); bottom left:
600 easterly continental flow (trajectory groups G5-G12).

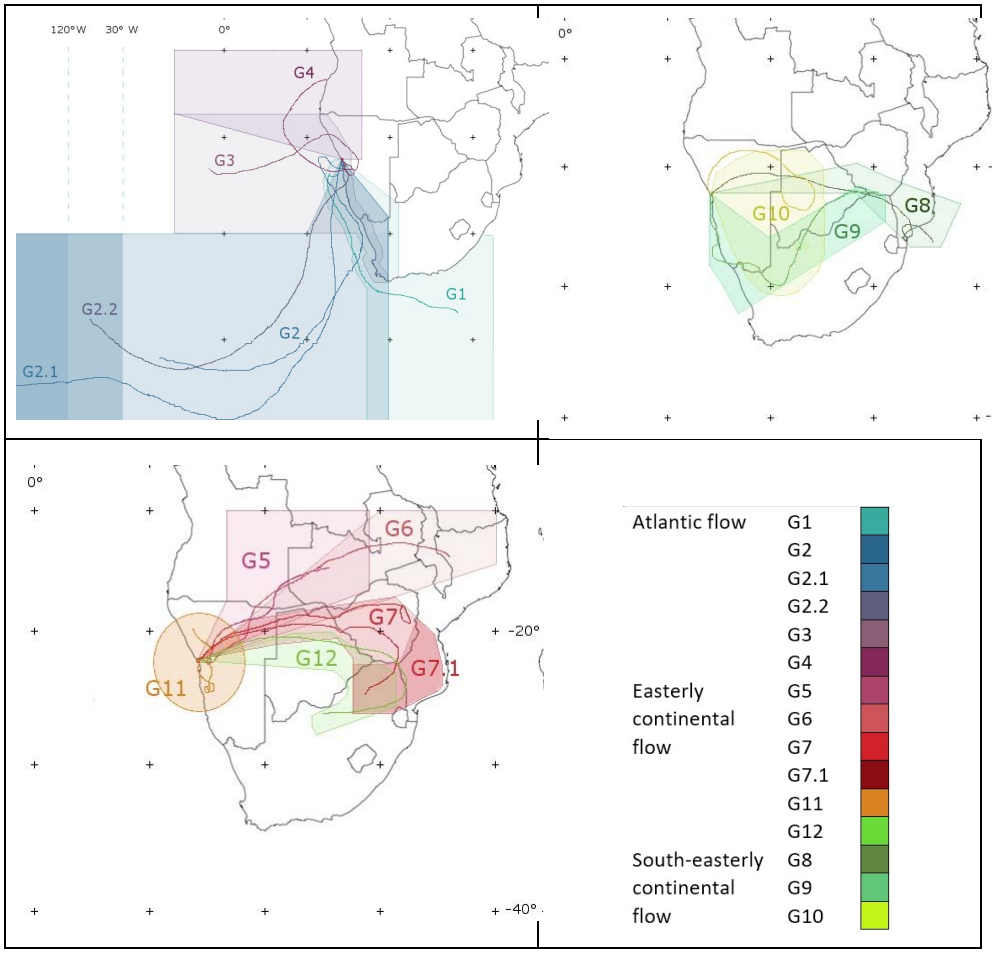

601

Atmos. Chem. Phys. Discuss., https://doi.org/10.5194/acp-2017-471
Manuscript under review for journal Atmos. Chem. Phys.
Discussion started: 6 June 2017

Atmospheric Chemistry and Physics Discussions

602 **Figure 4.** Yearly frequency distribution of trajectory pathways corresponding to BC_{eq} > 100 ng
603 m^{-3} in the Atlantic group (blue), south-easterly continental group (orange) and easterly
604 continental flow (grey) for the study period (July 2012-December 2015).

605
606

Atmos. Chem. Phys. Discuss., https://doi.org/10.5194/acp-2017-471
Manuscript under review for journal Atmos. Chem. Phys.
Discussion started: 6 June 2017

Atmospheric Chemistry and Physics Discussions

607 **Figure 5.** Box and whisker plot of the frequency distribution values of the excess mass
608 concentration of equivalent black carbon (excess eBC) measured for each flow path, Atlantic
609 (blue), south-easterly continental (orange), and easterly continental (grey), from left to right.
610 Boxes depict the 25%, the 50% (median) and the 75% percentiles. The open square represents
611 the mean of the distribution, whereas the whiskers represent the minimum and maximum values
612 of the distributions.

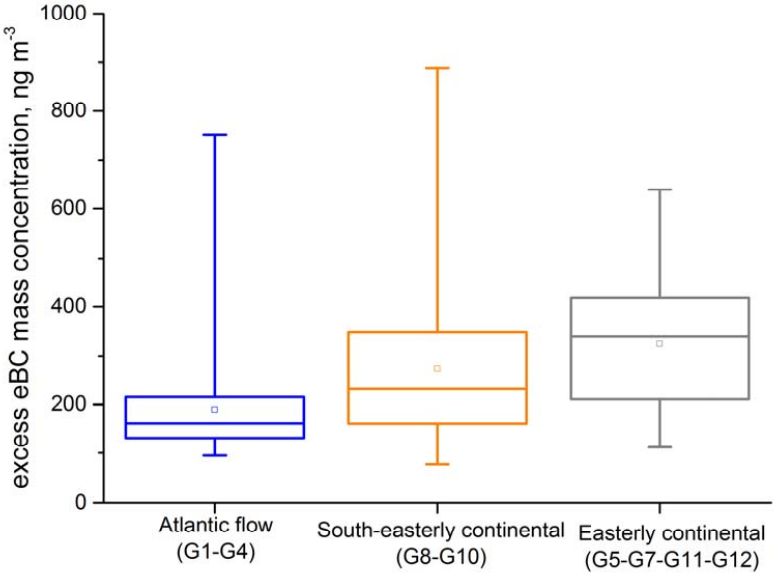

613
614
615
616